POLITECNICO DI TORINO
Repository ISTITUZIONALE

Feasibility study for reusing AlSi10Mg powder from the PBF-LB/M process in MAPS process

Original
Feasibility study for reusing AlSi10Mg powder from the PBF-LB/M process in MAPS process / Manfredi, D., Mercurio, V., Calignano, F., Arcieri, N., Marola, S., Lupoi, R., Iuliano, L.. - In: RESULTS IN ENGINEERING. - ISSN 2590-1230. - ELETTRONICO. - 28:(2025), pp. 1-11. [10.1016/j.rineng.2025.108055]

Availability:
This version is available at: 11583/3005736 since: 2025-12-09T16:13:51Z

Publisher:
Elsevier

Published
DOI:10.1016/j.rineng.2025.108055

Terms of use:

This article is made available under terms and conditions as specified in the corresponding bibliographic description in the repository

Publisher copyright

(Article begins on next page)

19 November 2026

Results in Engineering 28 (2025) 108055



Contents lists available at ScienceDirect

Results in Engineering

journal homepage: www.sciencedirect.com/journal/results-in-engineering



Feasibility study for reusing AlSi10Mg powder from the PBF-LB/M process in MAPS process

Diego Manfredi [a,b], Vincenza Mercurio [c], Flaviana Calignano [b,c,*], Nicolò Arcieri [a], Silvia Marola [d], Rocco Lupoi [e], Luca Iuliano [b,c]

[a] Department of Applied Science and Technology (DISAT), Politecnico di Torino, Corso Duca Degli Abruzzi, 24, 10129 Turin, Italy
[b] Integrated Additive Manufacturing Center (IAM), Politecnico di Torino, Corso Duca Degli Abruzzi, 24, 10129 Turin, Italy
[c] Department of Management and Production Engineering (DIGEP), Politecnico di Torino, Corso Duca Degli Abruzzi, 24, 10129 Turin, Italy
[d] Department of Mechanical Engineering, Politecnico di Milano, Via G. La Masa 1, Milano 20156, Italy
[e] Trinity College Dublin, The University of Dublin, Department of Mechanical, Manufacturing & Biomedical Engineering, Dublin, Ireland

ARTICLE INFO

Keywords:
Metal powder sheets
AlSi10 Mg
Reusing powder
Metal vaporization
Nanoindentation

ABSTRACT

Current research has explored the potential for producing powder sheets from AlSi10Mg powders considered as waste after laser-based powder bed fusion technology (PBF-LB/M). These sheets were then consolidated using novel metal additive manufacturing technique using powder sheets (MAPS). The use of Al based sheets is not yet well understood in literature, mainly due to the challenges posed by the material's properties, such as its high laser reflectivity and tendency to oxidize. The initial assessment of the feasibility of producing flexible Al-based sheets involved taking dimensional measurements and conducting electron and optical microscopy and thermal analyses. Twenty layers were consolidated onto aluminum substrates by varying two parameters: the angle of rotation between layers and the hatch distance. FESEM analysis revealed a uniform and very fine microstructure, comparable to AlSi10Mg single scan tracks (SSTs). According to the results of energy dispersive X-ray spectroscopy (EDX), the chemical composition of the sample was similar to that of the nominal AlSi10Mg alloy, except for the Mg content. Nanoindentation testing revealed an average hardness value of 2.1 GPa for the produced samples, surpassing those created using various rapid solidification methods.

1. Introduction

In the laser-based powder bed fusion for metals (PBF-LB/M) process, an additive manufacturing (AM) process, the interaction between the laser source and the powder bed during the melting process can result in several adverse phenomena, including spattering, metal vaporization, oxidation, agglomeration, and the partial melting of particles. As with other powder metallurgy processes, therefore, the choice of the proper powder is crucial to achieve the desired mechanical properties [1]. Several key elements, such as the powder characteristics, material contamination, and powder reuse, can significantly affect the quality of the finished products [2]. A notable advantage of the PBF-LB/M process is its ability to reuse powder remaining after component construction, enabling an economically sustainable approach by reducing waste. One of the most used materials in this process is the AlSi10Mg alloy, being one of the first aluminum alloys to be investigated [3]. Aluminum and its alloys are widely used in the automotive, aerospace, packaging, kitchenware, construction, electrical wiring, and other industries due to a range of properties like high strength-to-weight ratio and good corrosion resistance, excellent thermal and electrical conductivity and, most importantly, recyclability [4,5]. Kumar and Bharti [4] point out that annual aluminum consumption is estimated at around 60–80 million tons, with approximately 75 % coming from minerals. In contrast, aluminum scrap accounts for about 25 % of total annual demand. Recycling aluminum scrap presents a number of challenges. Traditional aluminum recycling methods result in significant material loss, largely due to metal oxidation during melting, the presence of slag, and additional waste generated during casting and processing. It is estimated that almost half of the materials are wasted with this conventional approach to recycling. On the other hand, powder metallurgy has established itself as a highly efficient technique for recycling metals and their alloys [4]. However, the process of reusing metal powder requires thorough evaluation and for example it is usually avoided in the production of biomedical implants in order to prevent contaminated

* Corresponding author.
E-mail address: flaviana.calignano@polito.it (F. Calignano).

https://doi.org/10.1016/j.rineng.2025.108055
Received 1 August 2025; Received in revised form 9 October 2025; Accepted 2 November 2025
Available online 3 November 2025
2590-1230/© 2025 The Author(s). Published by Elsevier B.V. This is an open access article under the CC BY-NC-ND license (http://creativecommons.org/licenses/by-nc-nd/4.0/).

implants and ensure a strict control on the chemical composition [6]. When considering the PBF-LB/M process, the disposal of metal powder requires specific processes [7], which can be costly given its classification as a hazardous material, mainly due to the mean size which is in the range 15–90 μm. The cost of disposal can vary significantly depending on the type and amount of powder and on the disposal method chosen, which may include recycling, hazardous waste management or industry-specific disposal services. Costs may include fees for specialized waste collection containers and transportation. Various scientific studies have shown the feasibility of reusing powder as long as the quality required for a given component is guaranteed. The ISO/ASTM F3456–22 standard [8] provides a set of powder reuse schemes for manufacturers, customers, and regulatory bodies with concise and clear terminology. Each scheme represents a broad reuse strategy and is intended as a starting point for managing powders in the whole PBF-LB/M process in order to reduce the risk of raw material contamination and associated defects within the manufacturer's quality management system.

After each PBF-LB/M cycle (called job), powder not used for manufacturing parts and therefore not melted and consolidated, may contain agglomerated particles [9–11]. These fine agglomerates are more likely to induce the formation of pores and voids during the production process due to the irregular shapes and variable sizes of the agglomerates formed [12]. Furthermore, when powders agglomerate, they affect the powder spreadability on the building platform, and tend to increase the reflectivity of the powder layer reducing the energy absorption during production [13]. Therefore, it is essential to implement procedures, such as sieving in order to reduce agglomerates [14], that guarantee an acceptable level of quality for the powders to be reused in subsequent part production using the PBF-LB/M process. Fully automated closed-loop solutions in an inert atmosphere for sieving and reusing powders have become increasingly popular in the industrial sector [15,16]. When the powder is reused, it can exhibit differences in particle size distribution, chemical composition, particle morphology and flow characteristics. A number of research efforts were conducted to examine the various impacts on metal powders collected from the build chamber following several rounds of recycling (up to over thirty times) [17–21]. There is a consensus that, after a certain number of recycling iterations, either the mechanical integrity of the printed component or the properties of the powder itself becomes problematic [22]. The main issues are heightened oxidation levels on the surface of the recycled powder and changes in particle size distribution. Fluctuations in the chemical composition of the particles can also result in significant discrepancies in the composition of the manufactured parts. Examining the impact of incorporating recycled powder on the microstructure and mechanical characteristics of the produced component is essential. This is especially vital in sectors like aerospace, where maintaining quality standards and consistency is mandatory.

Another aspect that has become increasingly important in industrial research in recent years is the handling and management of loose powders within the PBF-LB/M process chain. These powders pose a significant concern, particularly regarding the health and safety of operators, as well as the risk of fire and cross-contamination of materials. Inhaling finer particles during handling can lead to lung disease. At the same time, penetration of these particles through the skin may also lead to adverse health effects. Furthermore, cleaning machines after a building process and changing materials are labor-intensive activities that, depending on the material and the machine's dimensions, may take several working days [23]. To address the issues related to loose powders, a novel metal additive manufacturing technique using powder sheets (MAPS) was recently developed at Trinity College Dublin [24]. This process introduces the concept of a powder sheet, which represents a composite material, made by metallic powders and a polymeric binder, that replaces loose powder in PBF-LB/M. This flexible sheet differs from the solid foils used in the LOM process. Pre-production of the feedstock uses a solvent casting method similar to tape casting, employing Teflon as substrate. The build process then takes place in an inert atmosphere. Once the laser beam is activated, the polymeric binder vaporizes and the metal particles melt simultaneously. Once the predefined shape has been melted selectively, the laser turns off and the base plate lowers by a distance equal to the thickness of the solid material. A new section of the powder sheet then moves to cover the build platform. This process is repeated until the parts are fully formed [25]. As reported in the literature on this specific process [23–26], the MAPS system is still under development. Therefore, a modified PBF-LB/M system without a recoater but with a glove box could be used to create samples. This involves manually positioning one sheet on top of the other after melting each layer, while maintaining oxygen control below the threshold throughout the process. In terms of feedstock management and sustainability, using powder sheets offers several advantages: safe handling, storage and transportation of materials; ease of cleaning the building chamber; minimal material consumption; and reduced waste production due to the sheets being recyclable and reusable. Additionally, this technology could enable the use of irregular powders in size and shape, thereby reducing the cost of raw materials [27].

Starting from these considerations, this study focused on testing the feasibility of the MAPS process using AlSi10Mg powder which was no longer suitable for PBF-LB/M due to property degradation. Demonstrating this would mean to consolidate successfully such powder through this recently developed process giving also a possible alternative industrial route to handle them with reduced safety issues. To the authors' knowledge, the use of AlSi10Mg-based sheets has not yet been studied, primarily due to the challenges posed by this material's intrinsic properties, including high laser reflectivity and a high tendency to oxidize. Consequently, a high level of thermal energy is required for melting, which can cause numerous issues [28]. The feasibility of producing flexible and homogeneous AlSi10Mg-based sheets was first assessed using dimensional inspection, electron and optical microscopy, and finally thermal analysis. The most regular region of the sheets in terms of powder distribution and residual void content was then selected, and twenty layers cut from the sheets were consolidated on top of AlSi10Mg substrates. It was decided to kept laser power and scanning speed as fixed parameters, and to vary the rotation angle between subsequent layers and the hatching distance. Once obtained the lowest residual porosity through the proper combination of process parameters, the microstructure of the melted layers was investigated using optical and electron microscopy coupled with energy-dispersive X-ray (EDX) analysis. Finally, the mechanical response of such samples that are similar to Al-based coatings on AlSi10Mg substrates was evaluated using nanoindentation tests due to their relatively low thickness. These nanoindentation results were then compared with those obtained using the same instrument on AlSi10Mg samples produced using different rapid solidification techniques, such as melt spinning (MS) for ribbons, PBF-LB/M for single scan tracks (SSTs) and for cubic samples [29,30].

2. Materials and methods

2.1. AlSi10Mg based powder sheet production

The AlSi10Mg alloy powder (by EOS GmbH) employed for the creation of the powder sheets was considered as waste coming from the PBF-LB/M process. It was adopted the discrete reuse scheme according to ISO/ASTM F3456–22 (Fig. 1). The starting virgin powder had an average particle size distribution (PSD) of 25–70 μm [31]. The first job used virgin powder, whose bin was identified by a lot number. After the parts were produced, the used powder was sifted and stored in a container labeled "used" powder. In subsequent jobs, if there wasn't enough virgin powder to complete a production run, the powder was mixed with the "used" one. Each time batches of "used" powder were processed in a production run, a sequential designation ('*n*' in Fig. 1) was applied to track how many times the powder has been reused. This process was repeated until the powder lot was exhausted, there was insufficient used powder to complete an additional production run or

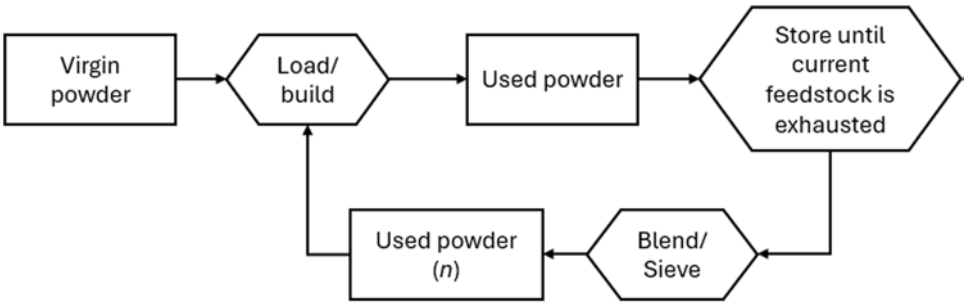


Fig. 1. Powder reuse scheme for "discrete reuse" according to ISO/ASTM F3456–22.

the powder no longer met the manufacturer's requirements.

The powder used to create the sheets was considered as waste for the PBF-LB/M process after 20 cycles (*n*) because it did not allow to obtain the desired as-built roughness values for the application required by the components produced with that batch. This powder had previously been used to create components for the aerospace industry, for which the same batch number was required as mandatory. Forty kilograms of AlSi10Mg powder were used for 20 jobs with an average component height of 110 mm ± 51 mm and an average job duration of 25 h ± 7 h. These standard deviation values are due to the fact that components with the same height but different cross-sectional dimensions have different times. However, after 20 jobs the powder was no longer able to produce components with a surface roughness of <10 μm. The roughness obtained in the first 18 jobs with the same process parameters that had been defined and qualified and therefore could not be modified according to the customer's requirements allowed values of 5 μm. Higher roughness values were therefore considered unacceptable.

The PSD of the waste powder was determined using a laser granulometry Mastersizer 3000 analyser, obtaining the following mean values: a D_{10} of 27 μm, a D_{50} of 46 μm and D_{90} of 76 μm. These percentile values indicate that 10 %, 50 % and 90 % of the particles are equal to or smaller than the corresponding size. These values are practically the same of the virgin powder, with a D_{10}, a D_{50} and a D_{90} of 24 μm, 44 μm and 74 μm respectively. Then the waste powder was investigated using a Zeiss Supra TM 40 field emission scanning electron microscope (FESEM) coupled with EDX analysis for chemical composition, which resulted in agreement with the EOS data sheet [31].

As can be seen in Fig. 2a, after 20 reuse cycles the powders are still almost spherical in shape, even considering the presence of some agglomerates and partially melted particles. However most of the largest particles had a bright appearance. This indicates a high level of surface oxidation. Zooming into one of these particles (Fig. 2b) reveals that they are the spattered ones from the different jobs. In fact they are covered by a sort of skin with a characteristic nodular oxide scale, which is formed during melting and solidification, as observed also by Raza et al. [32]. As visible in Fig. 2b, this aspect is may be due to a fragile rupture of the thin oxide layer induced by the particles impacting the surrounding environment.

For the fabrication of the AlSi10Mg powder sheet an in-house solvent casting machine developed at Trinity College Dublin [24] was employed. As in previous studies using other metallic alloys [24–28], the film-forming solution was prepared by initially dissolving polycaprolactone (PCL, $(C_6H_{10}O_2)_n$) pellets in a chloroform ($CHCl_3$) solvent and then mixing the solution with metallic powders. This mixture of metal, polymer and solvent was then deposited onto a Teflon substrate 60 μm thick (Fig. 3a). In this study, the doctor blade gap width of the tape casting system was set at 200 μm (i.e. the theoretical thickness of the powder sheet with Teflon). Once the $CHCl_3$ solvent had completely evaporated, the AlSi10Mg/PCL composite film solidified into a flexible powder sheet and was peeled off the Teflon foil (Fig. 3b).

The AlSi10Mg/PCL sheet was then characterized using a Laserliner coating thickness measuring instrument (Coating TestMaster, Mitutoyo). Since it could be slightly uneven, presenting areas with an irregular distribution of powders and residual voids, which could significantly impact the consolidation step with the laser, the sheet was extensively observed. To do this, the sheet was divided into three parts after a rapid visual inspection: one-third-of the total length was named the initial zone, one-third-the central zone, and one-third-the final zone.

Firstly, the sheet was analyzed using FESEM. Ten images were captured for each zone at 150x magnification, and a further five at 1000x magnification. However, it should be noted that this type of microscopy does not allow to determine with certainty whether the dark areas are related to the presence of the polymeric binder or to other metallic particles that are not visible due to the depth of field. Instead transmitted light illumination would be more useful for distinguishing the metal from the polymer; this method is typically employed to illuminate transparent samples from below using a backlight source. Consequently, the AlSi10Mg/PCL sheet was also characterized using a stereomicroscope in transmitted light mode. Twenty-five images were captured for each zone at 35x magnification. The percentage area in which only the polymer binder is present was estimated using ImageJ software for the analysis [33]. For each image, threshold of white and

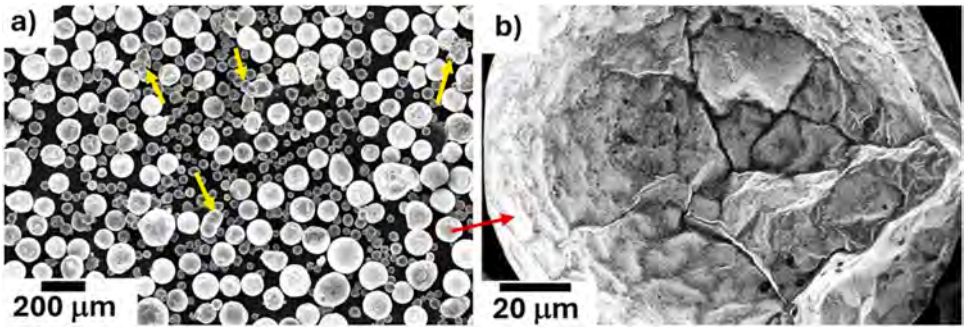


Fig. 2. FESEM images using In Lens detector of the AlSi10Mg waste powder employed in this study: (a) an overview, with yellow arrows indicating agglomerated particles and red arrow indicating (b) a magnification of a spattered particle.

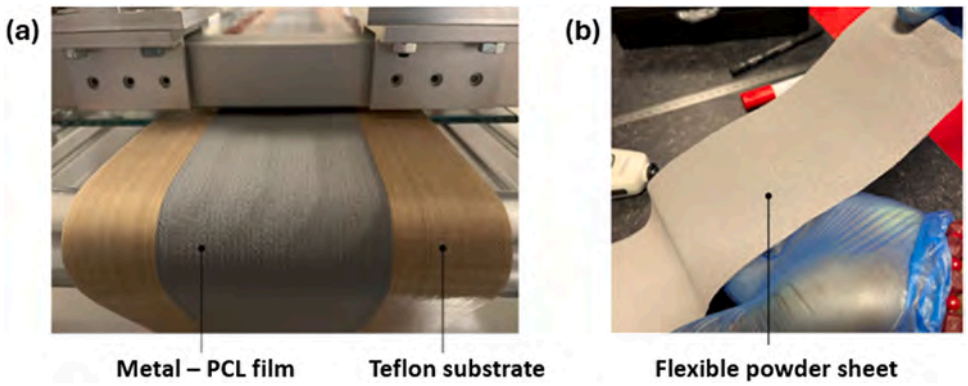


Fig. 3. Solvent casting (a) of the mixture AlSi10Mg/PCL on the Teflon substrate; (b) the AlSi10Mg/PCL flexible sheet removed from the substrate.

black pixels was established to define zones containing only polymer (white pixels) and zones containing both metal and polymer (black pixels). The outcome of this analysis was the selection of the sheet zone to undergo consolidation in the PBF-LB/M system.

Finally, a thermogravimetric analysis (TGA) was conducted on a selected zone of the sheet to investigate the thermal stability and the decomposition mechanism of the composite material [24–28]. The analysis was performed in an Ar atmosphere to simulate the environmental conditions during processing, with the sheet heated from ambient temperature to 700 °C at a rate of 10 °C/min.

2.2. Equipment for sheets consolidation

A selected zone of the AlSi10Mg/PCL sheet was cut in smaller portions prior to processing through a Print Sharp 250 commercial PBF-LB/M system, equipped with a Yb fiber laser with a nominal power of 500 W and a nominal focus diameter of 100 μm. The building process was conducted in an Ar atmosphere to keep the O_2 content below 0.1 % throughout manufacturing. The machine was adapted for processing the sheets by removing the recoating system. Furthermore, due to the absence of a roller mechanism to move the sheets, they were positioned manually over the building platform using the glove-box system of the machine after each laser exposure of a layer, as done in previous studies [24]. A modified aluminum building platform consisting of 40 mm diameter designed cavities that can host nine 10 mm thick metallic disks was utilized (Fig. 4a). Each disk can act as a substrate during the melting process and then it can be easily removed to allow microstructural characterizations [34]. The material of the disks should be as similar as possible to that of the sheets; therefore, AlSi10Mg disks (referred to simply as 'substrate' in the remainder of this study) were used in a T4 heat-treated state to avoid high residual stresses [35].

As can be seen in Fig. 4b, the sheet portions to be cut were handled through ring-shaped supports glued to them. As Zhang et al. observed in previous studies [24–27,36], sheets typically have two sides: a metal side and a polymer side. This is due to the solvent evaporation mechanism at the end of the film casting process (Figs. 4c and 4d). It was observed that placing the metal side adjacent to the platform (first layer) or to the melted material (subsequent layers) is preferable [24–28], and this approach was adopted.

2.3. Process parameters

The building platform was pre-heated up to 200 °C. During the process, twenty sheet layers were manually overlapped one at a time to print four 8 mm x 8 mm square samples on a AlSi10Mg-T4 disk, using a unique combination of process parameters each (Fig. 5).

Given the thickness of the powder sheets and considering previous studies [24–28], the platform was lowered by 90 μm after each laser exposition in these experiments. Two methods are generally used to identify the optimal process parameters window for the alloy under consideration: energy density and normalized enthalpy [37]. However, in the case of powder sheets, these are composites AlSi10Mg/PCL, which makes these two methods more difficult to use. The laser energy intensity and wavelengths differ between the polymer and the metal. The parameter window best suited to the polymer would not allow AlSi10Mg to melt. Since the polymer is used as a binder for metal powders, the starting point was to set the laser power (P) and scanning speed (v) identified as suitable for AlSi10Mg for a 90 μm layer in a previous study using the same PBF-LB/M system [38]: $P = 370$ W and $v = 1400$ mm/s, respectively. Production quality varies even if the energy input is the same. This difference in production quality is mainly due to the influence of the scanning speed on the hatch distance between adjacent melting pools. If the overlap rate of adjacent melting pools is adequate, the parts produced are dense and highly accurate. If, on the other hand, the hatch distance is too small, the fusion line would be too large due to excessive overlap; if the hatch distance is too large, the overlap between the melting pools is insufficient and the fusion line would appear to consist of discontinuous points. In the latter two cases, porosity could

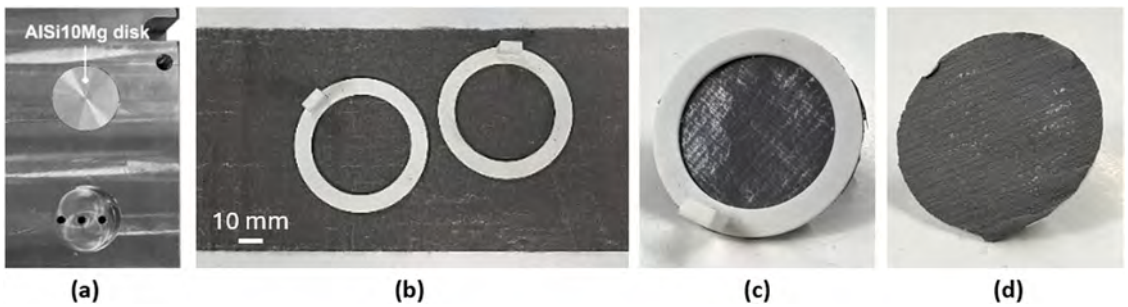


Fig. 4. (a) Image of a part of the modified building platform with one AlSi10Mg-T4 disk used as substrate in the present study, (b) ring-shaped supports, (c) polymer side and (d) metal side of the AlSi10Mg/PCL sheet.

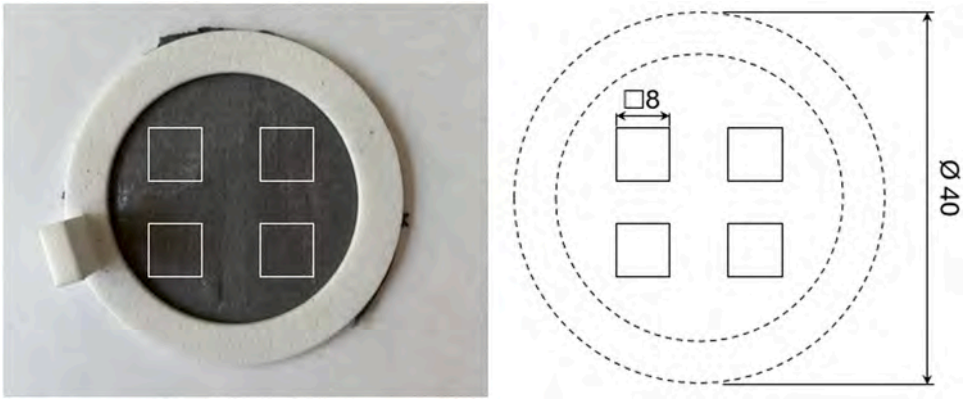


Fig. 5. Image and schematic representations of the square samples inside a disk in the ring-shaped support. Measurements are in millimeters.

occur inside the parts. Therefore, in order to determine the optimal process parameters, keeping the laser power and scanning speed constant, the effects of two hatching distances (h_d), 0.13 mm and 0.17 mm, and two rotation angles (α) between successive layers, 45° and 67°, were studied. These values were chosen on the basis of the literature since they generally allow for dense aluminum parts with reduced stress [39–42].

2.4. MAPS samples characterization

The initial investigation of the consolidated Al-based samples on the AlSi10Mg-T4 substrates was conducted through optical microscopy using a Leica DM6 M to determine the level of residual porosity employing different process parameters. Prior to analysis, the samples were cut parallel to the building direction. The cross-sections were ground using SiC paper up to 4000 grade, followed by polishing with diamond paste up to 1 μm, then end-polishing with a silica oxide suspension down to 0.25 μm. For each combination of process parameters, ten grayscale images at 200X magnification were acquired, and then processed employing ImageJ software [33]. Once defined the optimal process parameters, corresponding to the lowest residual porosity and to the most regular surface profile, the consolidated samples microstructure was investigated before and after etching with diluted Keller solution (20 % Keller 80 % H_2O for 10 s) using the Leica DM6 M and the Zeiss FESEM described previously. EDX analyses were also performed on un-etched samples to evaluate their chemical composition in comparison to the starting powder.

To provide a mechanical characterization of the Al-based samples obtained, nanoindentation was considered as it is the most suitable technique for very thin samples. The instrument used was a TI950 Hysitron nanoindenter, equipped with a Berkovich indenter tip, consisting of a three-sided diamond pyramid with an included angle of 142.3° and an angle of 65.35° from the normal to the face. The test conditions were chosen based on the previous works of Marola et al. [30, 43] on AlSi10Mg specimens produced using different rapid solidification techniques. A grid of 10 × 15 with 150 indentation marks, 7.5 μm apart, was created in the vertical cross-section to cover an extended area from the substrate to the upper part of the consolidated material. The loading-unloading speed was set to 100 μN/s, with a maximum load of 2.5 mN held constant for 5 s. The mean nanohardness values were determined from the loading-unloading curves using the Oliver and Pharr method [44]. According to this method the value of nanohardness can be estimated as follows (Eq. (1)):

$$H = P_{max}/A_c \quad (1)$$

where P is the applied maximum load, A_c is the projected area of contact.

Furthermore, the indentation marks were analysed again using the Zeiss Supra FESEM to highlight any differences that could be attributed to the microstructure.

3. Results and discussion

3.1. AlSi10Mg/PCL sheet characterization

The AlSi10Mg/PCL sheet produced by solvent casting method was 3.2 m long and 15 cm wide, with an average thickness of 117 ± 24 μm. As previously mentioned, the composite sheet was divided into three zones for analysis by microscopic observation. The FESEM micrographs in Fig. 6 show the distribution of powder particles across the sheet in each zone.

Fig. 6a shows that there are more small particles than large ones in the initial zone. In contrast, Fig. 6e shows that there are more large particles in the final zone. Therefore, the central zone of the sheet (Fig. 6c) exhibits a more even distribution of small and large powder particles. As can be seen at high magnification (Figs. 6b–d and f), the larger and smaller powder particles are held together by a continuous medium: the polymeric binder (PCL). The PCL appears as a thin film that uniformly coats and links the powder particles, thus determining the flexibility of the sheet. However, if there is a significant difference in size between the large and small particles, the polymer film tends to create crazes, as highlighted by the blue arrow in Fig. 6f.

Image analyses conducted in transmitted light mode using a stereomicroscope confirm the particles distribution, as can be seen in Fig. 7. Furthermore, a three-dimensional view of the three zones is provided, clearly distinguishing between dark/grey and light areas. The PCL is transparent to the light in the visible wavelength. Therefore, the dark/grey areas in the stereomicroscope images represent AlSi10Mg powders of different size linked by the polymer, whereas the light areas are related to the presence of the solely PCL. The biggest powder particles can be easily detected in light gray.

The percentage of polymeric binder Image analysis is 2.1 %, 1.5 % and 1.2 % in the initial, central and final zones, respectively. The presence of solely PCL areas could result in porosity and low densification levels in the printed parts. Consequently, utilizing the portion of the sheet with the lowest polymeric binder content could be advantageous. However, the differences between the central and final zones in terms of metallic voids are minimal. Additionally, the central zone appears more uniform, with a regular distribution of smaller and larger particles, as previously mentioned. Therefore, this zone of the sheet was selected for further thermal analysis. Fig. 8 shows the weight loss of the composite material as a function of temperature, representing the polymer's degradation performance by TGA. The analysis reveals that PCL degradation starts at 250 °C. Furthermore, when the temperature is higher than 350 °C, the TGA curves keep steady, showing that all the PCL binder has been fully degraded and only metal powder remains. The results show a total weight loss of 5.5 %, with an AlSi10Mg content of

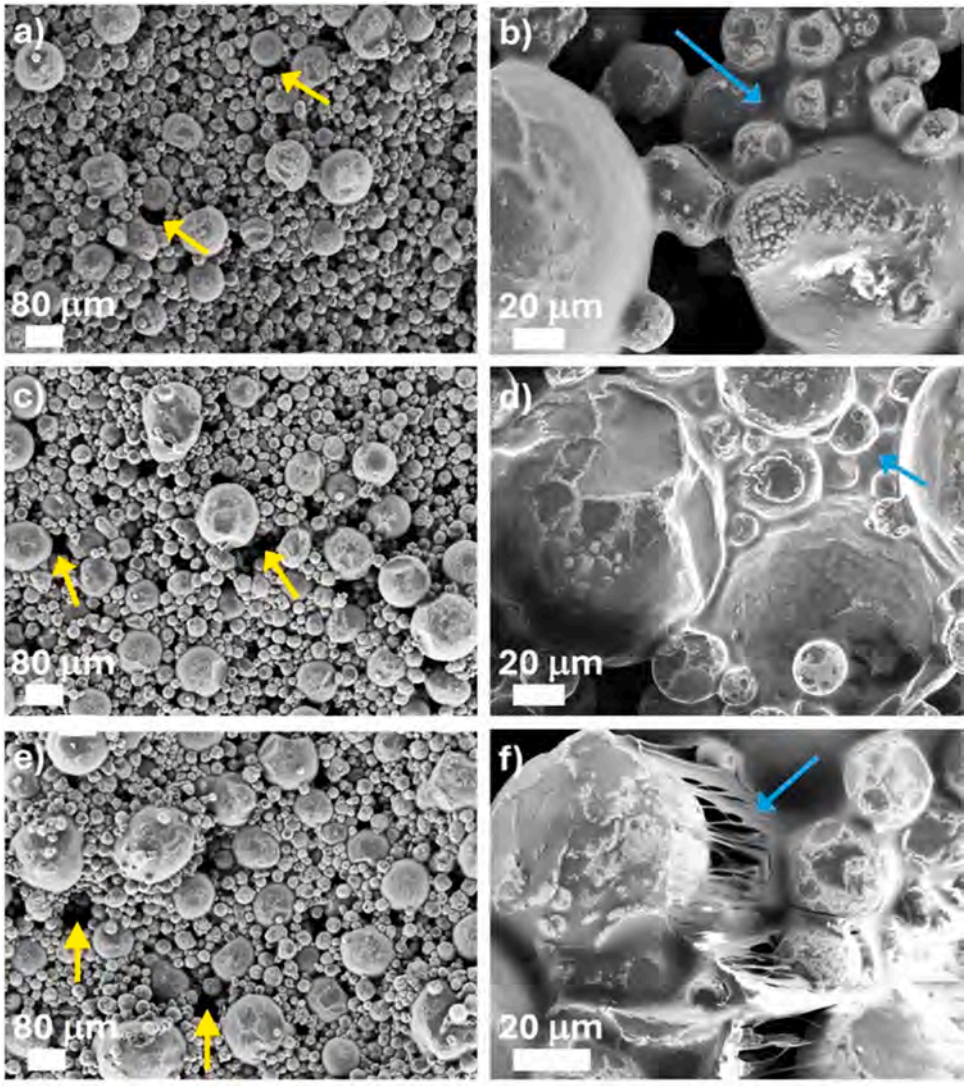


Fig. 6. FESEM images of the (a-b) initial zone, (c-d) central zone and (e-f) final zone of the AlSi10Mg/PCL sheet. In the low magnification micrographs with SE dectector (a-c-e), yellow arrows point to possible voids in the sheet, while in the high magnification micrographs (b-ᴅ-f) with In-Lens detector the blue arrows highlight the presence of PCL binder.

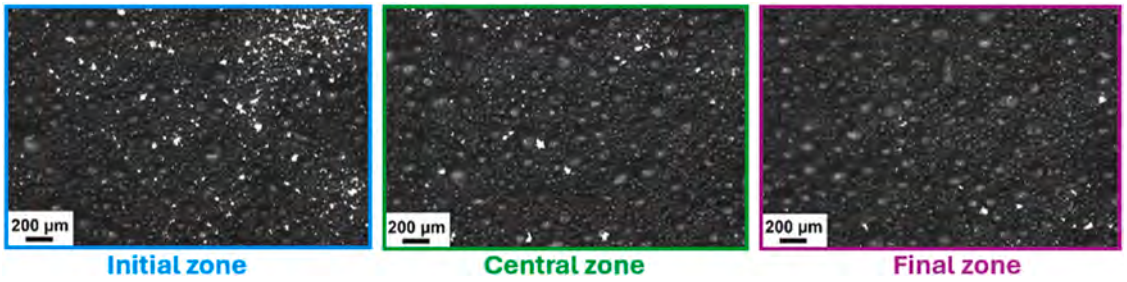


Fig. 7. Stereomicroscope images obtained in transmitted light mode of the initial, central and final zones of the AlSi10Mg/PCL sheet.

94.5 % wt in the composite sheet. These values are in agreement with previous studies based on other metallic alloys through MAPS process [24–28], indicating a high percentage of metallic powders. The central portion of the sheet was then selected to be cut in smaller portions using the ring-shaped supports.

3.2. Al-based samples characterization

Metallographic investigations of the Al-based samples using optical microscopy were firstly conducted to evaluate the impact of rotation angle and hatch distance on densification behavior. Table 1 reports the data of the relative density for each condition of process parameters employed.

As can be seen in the micrographs of Fig. 9, it is simple to distinguish

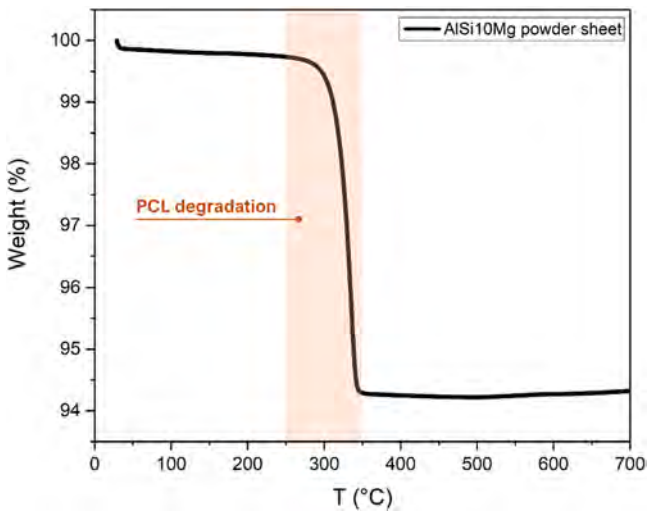


Fig. 8. TGA analysis of the central zone of AlSi10Mg/PCL sheet.

Table 1
Relative density measured by optical microscope for each process parameters combination of hatching distance and rotation angle.

		α	
		45°	67°
h_d	0.13 mm	96.87 % ± 1.57 %	95.84 % ± 1.76 %
	0.17 mm	98.05 % ± 0.96 %	93.34 % ± 2.29 %

the consolidated samples on top of the AlSi10Mg-T4 substrates. In fact it is well known that the AlSi10Mg alloy in this heat-treated state possesses a microstructure characterized by the presence of coarse globular Si micrometric precipitates within the Al matrix [34]. In the optical micrographs the matrix is the bright phase with dark grey Si particles. It can be stated that the consolidated Al-based material is well bonded to the substrate, even if it has an undulated profile due to the different penetration of subsequent laser scan tracks. In particular, looking at Fig. 9, samples manufactured with a rotation angle of 67° exhibits a greater number of pores, being mainly spherical gas porosity, than the samples produced with a rotation angle of 45° This could be attributed to the interaction between the direction of the shielding gas and the direction of the scan vectors. As observed in the PBF-LB/M process [37,45,46], certain scanning directions can generate more defects in the melting zone, such as spatter and porosity, than others. In the 67° scanning strategy, when the scanning direction coincides with the direction of the inert gas flow inside the chamber, although with differences of only a few degrees, the layer appears defective and the splashes that are created tend to settle in certain areas, producing defects [37]. The shape of the pores shows that they are mainly due to trapped gas, considering also the evaporation of the PCL binder during MAPS process [28].

On the other hand, it can be appreciated by both Table 1 and by looking at Figs. 9a-c the impact of hatch distance on densification and porosity in samples produced with a 45° rotation angle. The micrographs demonstrate also that the sample with a hatch distance of 0.17 mm has the most uniform and regular morphology regarding the upper surface of the consolidated layers.

Once the process window has been defined, the obtained samples were analyzed in terms of microstructure after chemical etching (Fig. 10). Thanks to Keller's reagent it is possible to appreciate the presence of the superimposing laser scan tracks, also called melt pools, confirming the explanation stated before about the undulated profile on top of the substrate. Moreover, going to high magnifications (Fig. 10b), also the very fine cellular network, typical of AlSi10Mg alloy after rapid solidification processes [29], could be detected.

Fig. 11 reports the EDX analysis performed on the Al-based sample to obtain a map of the elemental distribution of the main alloying elements in the consolidated material. The images of each color map show a homogeneous distribution of all the elements, taking into account also the very fine scale size of the microstructure, namely Al, Si, and Fe with weight percentages of 91.25 %, 8.47 % 0.29 % respectively. Even if it is known to be a qualitative analysis, this confirmed that the chemical composition of the Al-based sample obtained after MAPS process is close to that of the nominal AlSi10Mg alloy [31], albeit with a slightly lower percentage of Si.

On the other hand, the absence of Mg could be ascribed to the metal vaporization occurred during the MAPS process. As observed by Liu et al. in a comprehensive study on metal vaporization during PBF-LB/M [47], such physical process removes a large amount of heat from the

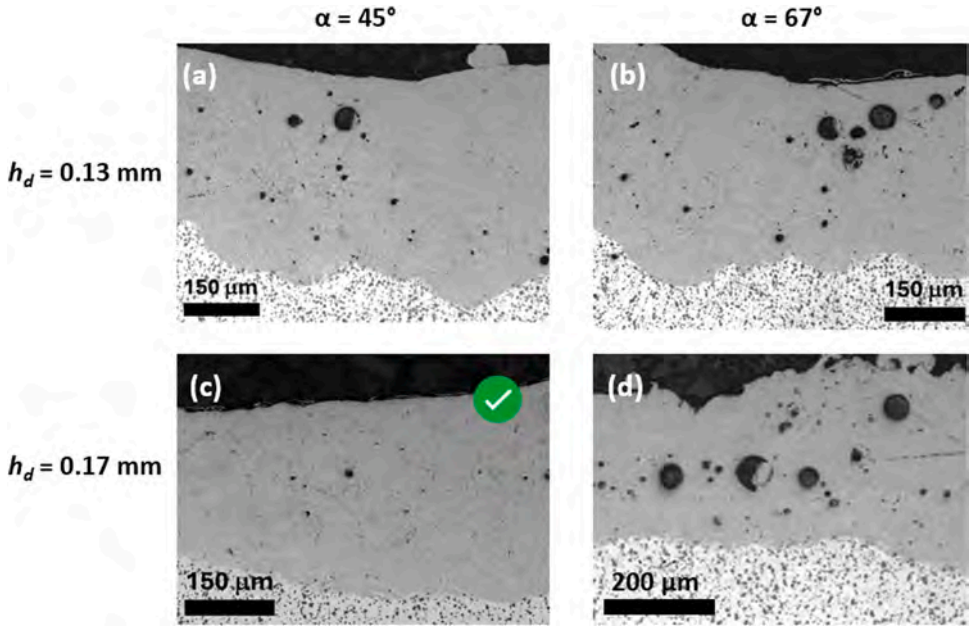


Fig. 9. Optical microscope micrographs of the vertical cross-section of the samples manufactured with the combination of process parameters reported.

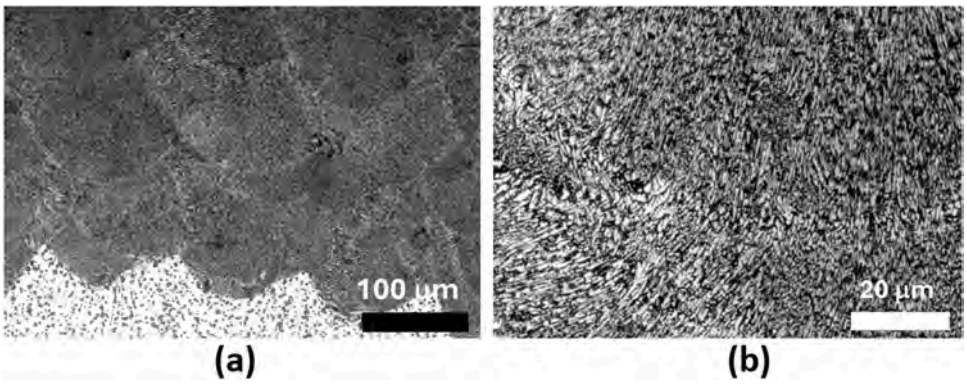


Fig. 10. Optical images of the microstructure after etching of the sample with the optimized process parameters: (a) superimposing laser scan tracks; (b) a magnification highlighting the extremely fine microstructure.

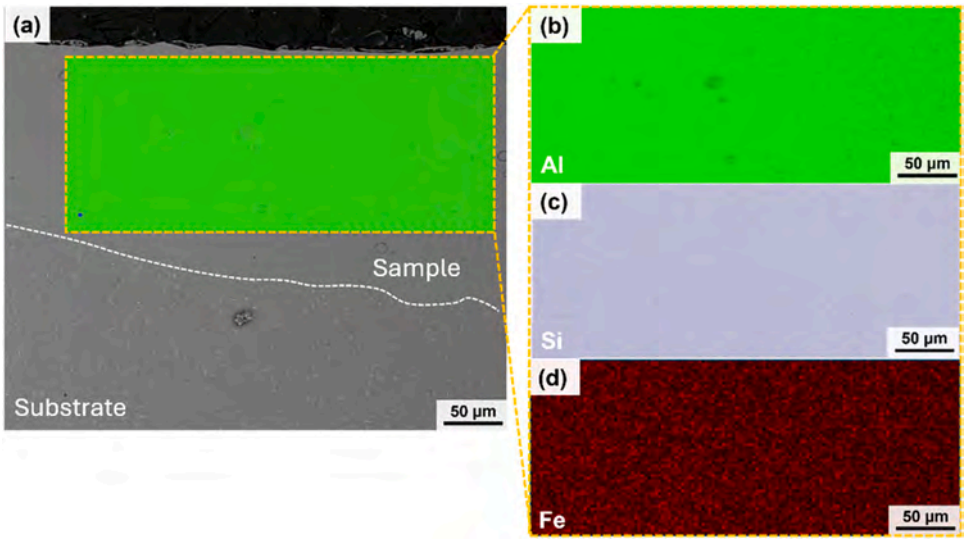


Fig. 11. FESEM-EDX elemental map analysis on a cross-section of the Al-based consolidated sample: (a) evidence of the area investigated, with (b) Al, (c) Si and (d) Fe distributions.

melt pool, because the latent heat of vaporization is more than ten times that of fusion, and leads to burning loss of elements. The authors state also that alloy parts produced by PBF-LB/M could exhibit a compositional change compared to the starting powder, particularly for alloys containing volatile elements such as Zn and Mg. For example a loss of Zn and Mg was observed by Wang et al. in a Al-Zn-Mg-Cu alloy [48]. The total vaporization loss occurs as follows: transportation of vaporization elements from the bulk to the surface of the melt pool, vaporization of elements at the liquid/vapor interface, and transportation of the vaporized species into the surrounding atmosphere. Mg has a high vaporization tendency, due to its low boiling point (T_b= 1091 °C) and low vaporization latent heat (ΔH = 134 KJ/mol) [46]. Moreover in the present study, the PCL binder evaporation that occurs during MAPS [28] could act as a further medium for Mg diffusion and transportation to the outer surface during melting.

The extremely fine microstructure was then investigated through FESEM on etched samples, as reported in Fig. 12a-f with progressive increasing magnifications. As in the case of optical microscopy, the Keller's reagent helped in highlighting the peculiar features. In the micrographs fine primary Al cells in grey are surrounded by fibrous eutectic which appears bright enhanced by the chemical etching. Looking at Fig. 12b, it can be seen a transition zone, no longer than few micrometers, in which the cells are coarser and elongated going from the consolidated sample to the substrate, where the globular micrometric dark grey Si particles are clearly visible. This change in size is due to the heat generated during subsequent laser scans and consequent repeated fusion. In Fig. 12d it is interesting to observe a peculiarity of the microstructure after MAPS process: some AlSi10Mg particles were not completely melted and could still be recognized, but they are fully integrated in the consolidated sample as demonstrated by the continuity of the eutectic network even through the outer borders of those particles. The primary Al cells are mainly equiaxed (Fig. 12c), and only in few regions of superimposition of different laser scan tracks they are slightly elongated due to the heat flux. In AlSi10Mg PBF-LB/M samples this happens in the melt pool borders, but in the case of Al-based samples by MAPS process the effect is really less pronounced. The explanations could refer to a different thermal history of the samples in this process: the powders are surrounded by a thin but continuous polymeric film, which is known to be a material with low thermal conductivity. This means that the materials undergo a different thermal history with respect PBF-LB/M in terms of heat conduction, contributing to a refining of the microstructure.

At high magnifications (Fig. 12e-f) the mean size of the equiaxed cellular structure could be obtained by image analysis. A mean value of 380 nm is associated to the Al-based sample after consolidation. Considering previous study by Marola et al. [30], this is the smallest value for primary Al cells, close to the one that can be obtained producing AlSi10Mg SSTs by PBF-LB/M.

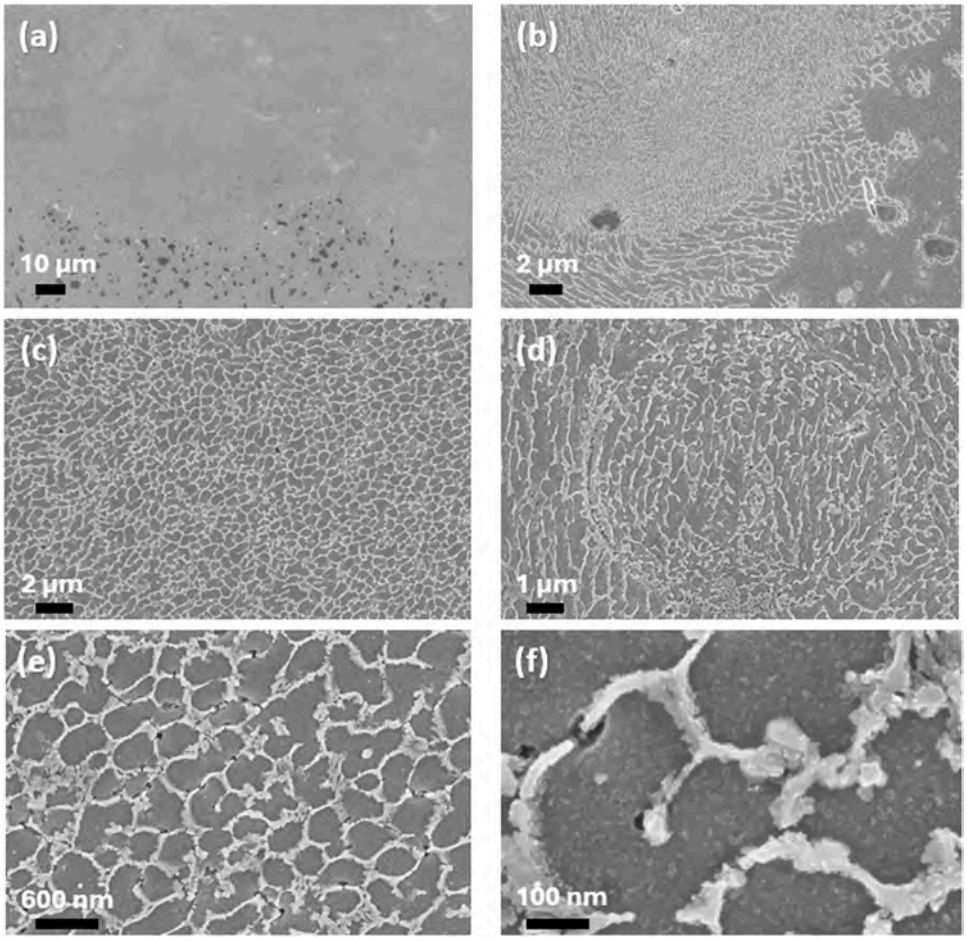


Fig. 12. FESEM images showing the microstructure of: (a) the Al-based sample and AlSi10Mg-T4 substrate; (b) a magnification of the transition zone between the consolidated sample and the substrate; (c) cellular equiaxed structure of the consolidated Al-based sample; (d) a magnification of cell structure with a AlSi10Mg particle embedded; (e) and (f) magnifications of the cellular equiaxed structure.

To assess the mechanical behavior of the Al-based samples, nanoindentation measurements were performed on an extended area to evaluate the mechanical performance of both the substrate and the upper part of the consolidated material. These measurements were then compared with those obtained using the same instrument on other AlSi10Mg samples produced by rapid solidification processes, including ribbons manufactured by the melt spinning (MS) process [29], laser single scan tracks (SSTs) and cubic samples by PBF-LB/M [31].

The mean nanohardness values are summarized in Table 2. As reported in the literature, a significant increase in hardness has been observed in the additively manufactured samples compared to the heat treated substrate and also compared to MS ribbons. Furthermore, the results reveal that the average nanohardness value of the Al-based samples in this study is slightly higher than that of bulk PBF-LB/M samples, with a lower standard deviation. This confirms that the material is dense and uniform with an extremely fine microstructure.

Further information can be obtained by inspecting the microstructure behind the nanoindentation grid using again FESEM analysis (Fig. 13). The hardness of the material increases when moving from the substrate to the sample, as indicated by the reduced size of the indentation marks. An increase in the hardness of the substrate can be observed only when measurements are taken in proximity to micrometer-sized Si precipitates and Fe-rich platelets [35].

Table 2
Hardness from nanoindentation for AlSi10 based alloy produced using different manufacturing techniques.

	Nanoindentation hardness [GPa]
Al-based sample – this study	2.1 ± 0.2
AlSi10Mg substrate – this study	1.7 ± 0.4
AlSi10Mg PBF-LB/M [30]	2.0 ± 0.2
AlSi10Mg MS [30,44]	1.8 ± 0.3
AlSi10Mg SST [30]	2.1 ± 0.1

4. Conclusions

The results obtained highlight the feasibility of reusing waste AlSi10Mg powders from PBF-LB/M process in another AM process, the MAPS process recently developed at Trinity College. The most significant achievements are summarized below:

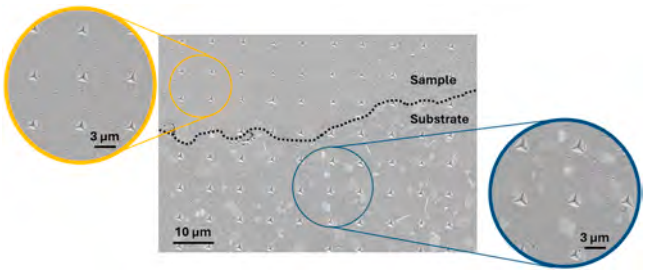


Fig. 13. FESEM images showing the nanoindentation grid in the analyzed area of the Al-based sample (in yellow) and of the AlSi10Mg-T4 substrate (in blue).

- An AlSi10Mg/PCL flexible and uniform sheet with a low percentage of voids could be obtained; TGA analysis indicated that the polymeric binder decomposes completely, leaving a metallic content of 95.5 % wt, therefore suitable for MAPS process.
- Al-based consolidated samples were obtained employing laser power of 370 W, scan speed of 1400 mm/s, hatch distance of 0.17 mm and rotation angle of 45° between successive layers. These parameters were optimized to ensure the lowest residual porosity (small gas spherical pores) and a perfect adhesion to the substrate.
- EDX results showed that the chemical composition of the Al-based samples was close to that of the nominal AlSi10Mg alloy apart from the Mg content. This is probably due to metal vaporization occurring during the consolidation of the layers, accompanied by the decomposition of the polymeric binder.
- Optical and FESEM analysis after chemical etching revealed an extremely fine microstructure, constituted by primary Al cells surrounded by fibrous eutectic; the cells are mainly equiaxed with a mean value of 380 nm, similar to the one that can be obtained producing SSTs by PBF-LB/M.
- Nanoindentation results showed a high mean hardness value of 2.1 GPa for the Al-based samples obtained; in comparison with other rapid solidification techniques, this is the highest nanohardness achievable starting from AlSi10Mg powders. Moreover, the low standard deviation confirmed the homogeneity of the extremely fine microstructure.

CRediT authorship contribution statement

Diego Manfredi: Writing – review & editing, Writing – original draft, Validation, Methodology, Investigation, Formal analysis. **Vincenza Mercurio:** Writing – original draft, Validation, Investigation, Formal analysis. **Flaviana Calignano:** Writing – review & editing, Writing – original draft, Visualization, Validation, Supervision, Methodology. **Nicolò Arcieri:** Writing – review & editing, Validation, Investigation, Formal analysis. **Silvia Marola:** Writing – review & editing, Formal analysis, Investigation, Validation. **Rocco Lupoi:** Resources, Conceptualization. **Luca Iuliano:** Supervision, Resources.

Declaration of competing interest

The authors declare that they have no known competing financial interests or personal relationships that could have appeared to influence the work reported in this paper.

Acknowledgements

The authors are grateful acknowledge the funding of PoSAddive – Powder Sheet Additive Manufacturing (EIT RawMaterials, No. 22021), and Enterprise Ireland (CF-2020–1564-A/B)

Data availability

No data was used for the research described in the article.

References

[1] S. Vock, B. Klöden, A. Kirchner, T. Weißgärber, B. Kieback, Powders for powder bed fusion: a review, Prog. Addit. Manuf. (2019), https://doi.org/10.1007/s40964-019-00078-6.
[2] G. Calignano, A metal powder bed fusion process in industry: qualification considerations, Machines 7 (2019) 72, https://doi.org/10.3390/machines7040072.
[3] F. Trevisan, F. Calignano, M. Lorusso, J. Pakkanen, A. Aversa, E.P. Ambrosio, et al., On the selective laser melting (SLM) of the AlSi10Mg alloy: process, microstructure, and mechanical properties, Materials (2017), https://doi.org/10.3390/ma10010076.
[4] N. Kumar, A. Bharti, Review on powder metallurgy: a novel technique for recycling and foaming of aluminium-based materials, Powder Metall. Met. Ceram. (2021), https://doi.org/10.1007/s11106-021-00214-4.
[5] S. Al-Alimi, N.K. Yusuf, A.M. Ghaleb, M.A. Lajis, S. Shamsudin, W. Zhou, et al., Recycling aluminium for sustainable development: a review of different processing technologies in green manufacturing, Results. Eng. 23 (2024) 102566, https://doi.org/10.1016/J.RINENG.2024.102566.
[6] M.A. Obeidi, Metal additive manufacturing by laser-powder bed fusion:guidelines for process optimisation, Results. Eng. 15 (2022) 100473, https://doi.org/10.1016/j.rineng.2022.100473.
[7] ISO/ASTM, Additive manufacturing of metals— Feedstock materials — Powder life cycle management n.d, 52928, https://www.iso.org/obp/ui/en/#iso:std:iso-astm:52928:ed-1:v1:en, 2024. accessed September 1, 2025.
[8] Standard guide for powder reuse schema in powder bed fusion processes for medical applications for additive manufacturing feedstock materials 2022. https://doi.org/10.1520/F3456-22.
[9] L. Cordova, M. Campos, T. Tinga, Revealing the effects of powder reuse for selective laser melting by powder characterization, JOM (2019), https://doi.org/10.1007/s11837-018-3305-2.
[10] L.C. Ardila, F. Garciandia, J.B. González-Díaz, P. Álvarez, A. Echeverria, M. M. Petite, et al., Effect of IN718 recycled powder reuse on properties of parts manufactured by means of selective Laser melting. Phys, Procedia (2014), https://doi.org/10.1016/j.phpro.2014.08.152.
[11] N.E. Gorji, R. O'Connor, D. Brabazon, XPS, XRD, and SEM characterization of the virgin and recycled metallic powders for 3D printing applications, IOP. Conf. Ser. Mater. Sci. Eng. (2019), https://doi.org/10.1088/1757-899x/591/1/012016.
[12] E.J.R. Parteli, T. Pöschel, Particle-based simulation of powder application in additive manufacturing, Powder. Technol. (2016), https://doi.org/10.1016/j.powtec.2015.10.035.
[13] C.D. Boley, S.A. Khairallah, A.M. Rubenchik, Calculation of laser absorption by metal powders in additive manufacturing, Addit. Manuf. Handb. Prod. Dev. Def. Ind. (2017), https://doi.org/10.1201/9781315119106.
[14] C. Gallagher, S. Nikam, E. Kerr, S. McFadden, Shape characterisation for mounted additive manufacturing powders, Results. Eng. 27 (2025) 106605, https://doi.org/10.1016/J.RINENG.2025.106605.
[15] R. Groarke, R.K. Vijayaraghavan, D. Powell, A. Rennie, D. Brabazon, Powder Characterization-Methods, Standards, and State of the Art, Elsevier Inc., 2021, https://doi.org/10.1016/B978-0-12-824090-8.00006-8.
[16] D. Powell, A.E.W. Rennie, L. Geekie, N. Burns, Understanding powder degradation in metal additive manufacturing to allow the upcycling of recycled powders, J. Clean. Prod. 268 (2020) 122077, https://doi.org/10.1016/j.jclepro.2020.122077.
[17] T. Fedina, F. Belelli, G. Lupi, B. Brandau, R. Casati, R. Berneth, et al., Influence of AlSi10Mg powder aging on the material degradation and its processing in laser powder bed fusion, Powder. Technol. (2022), https://doi.org/10.1016/j.powtec.2022.118024.
[18] P. Moghimian, T. Poirié, M. Habibnejad-Korayem, J.A. Zavala, J. Kroeger, F. Marion, et al., Metal powders in additive manufacturing: a review on reusability and recyclability of common titanium, nickel and aluminum alloys, Addit. Manuf. (2021), https://doi.org/10.1016/j.addma.2021.102017.
[19] M. Lutter-Günther, C. Gebbe, T. Kamps, C. Seidel, G. Reinhart, Powder recycling in laser beam melting: strategies, consumption modeling and influence on resource efficiency, Prod. Eng. (2018), https://doi.org/10.1007/s11740-018-0790-7.
[20] H. Asgari, C. Baxter, K. Hosseinkhani, M. Mohammadi, On microstructure and mechanical properties of additively manufactured AlSi10Mg_200C using recycled powder, Mater. Sci. Eng. A (2017), https://doi.org/10.1016/j.msea.2017.09.041.
[21] N.E. Gorji, P. Saxena, M. Corfield, A. Clare, J.P. Rueff, J. Bogan, et al., A new method for assessing the recyclability of powders within Powder Bed Fusion process, Mater. Charact. (2020), https://doi.org/10.1016/j.matchar.2020.110167.
[22] Weiss C., Munk J., Haefner C.L. Investigation towards AlSi10Mg powder recycling behavior in the LPBF process and its influences on mechanical properties 2021. https://doi.org/10.26153/TSW/17605.
[23] D.W. Gibbons, P. Govender, A.F. van der Merwe, Metal powder feedstock evaluation and management for powder bed fusion: a review of literature, standards, and practical guidelines, Prog. Addit. Manuf. 9 (2024) 805–833, https://doi.org/10.1007/s40964-023-00484-x.
[24] R. Lupoi, W.M. Abbott, R. Senthamaraikannan, S. McConnell, J. Connolly, S. Yin, et al., Metal additive manufacturing via a novel composite material using powder and polymers formed in sheets, CIRP Ann. 71 (2022) 181–184, https://doi.org/10.1016/j.cirp.2022.03.012.
[25] W. Zhang, S. Marola, S. McConnell, Z. Cai, J.M. Dugenio, M. Li, et al., Demonstration and benchmarking of a novel powder sheet additive manufacturing approach with austenitic steel, Mater. Des. 245 (2024) 113301, https://doi.org/10.1016/J.MATDES.2024.113301.
[26] W. Zhang, X. Lu, A. Coban, M. Cervera, M. Chiumenti, A. Sasnauskas, et al., Powder sheet additive manufacturing of multi-material structures: experimental and computational characterizations, Compos. B Eng. 272 (2024) 111203, https://doi.org/10.1016/j.compositesb.2024.111203.
[27] W. Zhang, A. Coban, A. Sasnauskas, Z. Cai, B. Gillham, W. Mirihanage, et al., A novel powder sheet laser additive manufacturing method using irregular morphology feedstock, CIRP. J. Manuf. Sci. Technol. 52 (2024) 26–35, https://doi.org/10.1016/j.cirpj.2024.05.007.
[28] J. Volpp, W. Zhang, W. Abbott, A. Coban, S. McConnell, S. Marola, et al., Binder evaporation during powder sheet Additive Manufacturing, in: 2023 Int Solid Free Fabr Symp, 2023, pp. 2271–2281.
[29] S. Marola, D. Manfredi, G. Fiore, M.G. Poletti, M. Lombardi, P. Fino, et al., A comparison of selective laser melting with bulk rapid solidification of AlSi10Mg alloy, J. Alloys. Compd. (2018), https://doi.org/10.1016/j.jallcom.2018.01.309.

[30] S. Marola, D. Gianoglio, F. Bosio, A. Aversa, M. Lorusso, D. Manfredi, et al., Alloying AlSi10Mg and Cu powders in laser Single Scan Tracks, melt spinning, and Laser Powder Bed Fusion, J. Alloys. Compd. 821 (2020) 153538, https://doi.org/10.1016/j.jallcom.2019.153538.
[31] EOS GmBH, EOS Aluminium, Material_Datasheet_EOS_Aluminium_AlSi10Mg_EN 2025, https://www.eos.info/it/var/assets/05-datasheet-images/Assets_MDS_Metal/EOS_Aluminium_AlSi10Mg/Material_Datasheet_EOS_Aluminium_AlSi10Mg_EN.pdf?v=6, 2025. accessed July 30.
[32] A. Raza, T. Fiegl, I. Hanif, A. MarkstrÖm, M. Franke, C. Körner, et al., Degradation of AlSi10Mg powder during laser based powder bed fusion processing, Mater. Des. (2021), https://doi.org/10.1016/j.matdes.2020.109358.
[33] S. Preibisch, S. Saalfeld, P. Tomancak, Globally optimal stitching of tiled 3D microscopic image acquisitions, Bioinformatics. (2009), https://doi.org/10.1093/bioinformatics/btp184.
[34] A. Aversa, M. Moshiri, E. Librera, M. Hadi, G. Marchese, D. Manfredi, et al., Single scan track analyses on aluminium based powders, J. Mater. Process. Technol. (2018), https://doi.org/10.1016/j.jmatprotec.2017.11.055.
[35] V. Drossou-Agakidou, F. Kanakoudi-Tsakalidou, K. Sarafidis, A. Taparkou, V. Tzimouli, H. Tsandali, et al., ASM Handbook Volume 2: Properties and Selection: Nonferrous Alloys and Special-Purpose Materials, ASM International Handbook Committee, 1990. Eur J Pediatr.
[36] W. Zhang, A. Sasnauskas, A. Coban, S. Marola, R. Casati, S. Yin, et al., Powder sheets additive manufacturing: principles and capabilities for multi-material printing, Addit. Manuf. Lett. 8 (2024) 100187, https://doi.org/10.1016/j.addlet.2023.100187.
[37] F. Calignano, A. Bove, M. Pavese, Processing of pure copper by powder bed fusion with infrared laser, Results. Eng. 25 (2025) 104497, https://doi.org/10.1016/J.RINENG.2025.104497.
[38] V. Mercurio, F. Calignano, L. Iuliano, Sustainable production of AlSi10Mg parts by laser powder bed fusion process, Int. J. Adv. Manuf. Technol. 125 (2023) 3117–3133, https://doi.org/10.1007/s00170-023-11004-0.
[39] N. Limbasiya, A. Jain, H. Soni, V. Wankhede, G. Krolczyk, P. Sahlot, A comprehensive review on the effect of process parameters and post-process treatments on microstructure and mechanical properties of selective laser melting of AlSi10Mg, J. Mater. Res. Technol. (2022), https://doi.org/10.1016/j.jmrt.2022.09.092.
[40] J.H. Robinson, I.R.T. Ashton, E. Jones, P. Fox, C. Sutcliffe, The effect of hatch angle rotation on parts manufactured using selective laser melting, Rapid. Prototyp. J. (2019), https://doi.org/10.1108/RPJ-06-2017-0111.
[41] P. Yadav, O. Rigo, C. Arvieu, E. Lacoste, Microstructural and mechanical aspects of AlSi7Mg0.6 alloy related to scanning strategies in L-PBF, Int. J. Adv. Manuf. Technol. (2022), https://doi.org/10.1007/s00170-022-09127-x.
[42] M. Tang, P.C. Pistorius, Oxides, porosity and fatigue performance of AlSi10Mg parts produced by selective laser melting, Int. J. Fatigue (2017), https://doi.org/10.1016/j.ijfatigue.2016.06.002.
[43] S. Marola, G. Fiore, L. Battezzati, Effect of modifiers on the microstructure of rapidly solidified AlSi10Mg alloy, Metall. Mater. Trans. a Phys. Metall. Mater. Sci. 54 (2023) 624–633, https://doi.org/10.1007/s11661-022-06907-8.
[44] W.C. Oliver, G.M. Pharr, An improved technique for determining hardness and elastic modulus using load and displacement sensing indentation experiments, J. Mater. Res. (1992), https://doi.org/10.1557/jmr.1992.1564.
[45] A.A. Bin, P. QC, Selective laser melting of AlSi10Mg: effects of scan direction, part placement and inert gas flow velocity on tensile strength, J. Mater. Process. Technol. 240 (2017) 388–396, https://doi.org/10.1016/j.jmatprotec.2016.10.015.
[46] Z. Liu, Y. Yang, D. Wang, Z. Chen, W. Yan, Correlation between the scan strategy, residing spatter distribution, and parts quality in laser powder bed fusion, Mater. Des. (2023), https://doi.org/10.1016/j.matdes.2023.112317.
[47] J. Liu, P. Wen, Metal vaporization and its influence during laser powder bed fusion process, Mater. Des. (2022), https://doi.org/10.1016/j.matdes.2022.110505.
[48] P. Wang, H.C. Li, K.G. Prashanth, J. Eckert, S. Scudino, Selective laser melting of Al-Zn-Mg-Cu: heat treatment, microstructure and mechanical properties, J. Alloys. Compd. (2017), https://doi.org/10.1016/j.jallcom.2016.11.210.